# Chapter 6

# A generalized viscous model governing tornado dynamics: An exact solution

## 6.1 Introduction

A tornado is a fast whirling columnar vortex wind system hanging as a pendent from a cumuliform cloud in contact with the surface of the earth. It is witnessed as a funnel merging into clouds with circulating dust at the foot. This low pressure visual core vortex rotating with terrific energy also travels along the ground surface. It is the most violent and destructive atmospheric vortex on the surface of the Earth. It is observed all over the world such as in Japan, Bangladesh, Britain, Australia,

The contents of this chapter are published in Zeitschrift für Naturforschung A, 73(8), 753-766, (2018).

but in large number in Tornado Alley in the USA. It is generally believed that the circulation of a tornado vortex is maintained by the rotating mother cloud and the sense of the vortex rotation coincides with that of the associated mother cloud (Ying and Chang, 1970).

Numerous theoretical and empirical models are available in the literature. The tangential velocity in tornadoes are generally approximated by continuous functions that are zero at the centre of the tornado, increase to a maximum at some radial distance, and then decrease asymptotically to zero at points infinitely distant from the centre. Different forms of the tangential component of velocity have been proposed with idealized Rankine (1882) combined vortex model as a first approximation. However, due to the absence of the radial and vertical components of velocity, Rankine combined vortex model is doubtfully a good approximation.

In the literature, a number of analytical, empirical and numerical models are available discussing the flow field of mature tornado-like vortices for single-cells and two-cells above the tornado boundary layer. Burgers (1948) and Rott (1958) both individually presented exact solution of full Navier-Stokes equations for viscous incompressible steady flow of a vortex with the radial velocity as $u = -ar$ ($a$ being the constant of proportionality), the azimuthal velocity $v = \Gamma\left(1 - \exp\left(-(ar^2)/2\nu\right)\right)/2\pi r$ ($\Gamma$ being the circulation and $\nu$ the kinematic viscosity), and the axial velocity $w = 2az$. While the azimuthal velocity has been found to fit well to some observed and experimental data by several researchers (Wood and Brown, 2011; Kim and Matsui, 2017; Gillmeier et al., 2018 etc.), the model may not be useful due to the fact that other components of velocity are unbounded. Other models available in the literature are either empirical or are unable to model a real tornado.

Sullivan (1959) gave an exact solution with some similarity to the Burgers-Rott vortex model. He discussed both one-celled and two-celled vortices. The two-celled vortex possesses an inner cell in which wind descends from above and flows outward to meet a separate wind that converges radially. Both the winds rise at the meeting point. The Sullivan vortex is a very simple vortex but can describe the flow in an intense tornado having a central downdraft and also its updraft is localized to a place meant for the thunderstorm. The axial pressure gradient however increases vertically without bound. Two-cell analytical Sullivan (1959) vortex model for steady incompressible viscous flow is quite complex.

Kuo (1971) analytically modeled the three-dimensional flow in the boundary layer of a tornado-like vortex and alternatively solved the two nonlinear boundary-layer equations for the radial and vertical velocities. The Bloor and Ingham (1987) vortex model and the Vyas-Majdalani (2003) vortex model are exact solutions for inviscid flows using the Euler's equations respectively in a conical and a cylindrical domain. Xu and Hangan (2009) used a free narrow jet solution combined with a modified Rankine vortex to analytically model an inviscid tornado-like vortex. However, the combined model is not an exact solution to the Navier-Stokes-Equations. Wood and White (2011) reported a new parametric model of vortex tangential-wind profiles, which is based on the Vatistas et al. (1991) model and is mainly designed to represent realistic-looking tangential wind profiles observed in atmospheric vortices.

Tornado-like flow field has been studied experimentally and/or numerically in numerous reports. A few of them are as follows: Ward (1972) simulated in a laboratory system the three features of tornadoes, viz., characteristic surface pressure profile, bulging deformation on the vortex core and multiple vortices in a single convergence system; Church et al. (1979) discussed the dynamics of natural tornadoes based on laboratory simulations; Lewellen et al. (1997) simulated tornado's

interaction with the surface; Natarajan (2012) discussed large eddy simulations of translation and surface roughness effects on tornado-like vortices; Sabareesh et al. (2012) too discussed surface pressure and surface roughness, whereas Liu and Ishihara (2016) studied translation and roughness on tornado-like vortices; Haan et al. (2008) designed a large tornado simulator for wind engineering applications; Mishra et al. (2008) physically simulated single cell tornado like vortex; Refan et al. (2014) tried to reproduce tornadoes in laboratory using proper scaling; Gillmeier et al. (2016) analysed influence of tornado generator's geometry on the flow field; Nolan et al. (2017) worked on tornado vortex structure, intensity and surface wind gusts in large eddy-simulations and Tang et al. (2018) worked on characteristics of tornado-like vortex simulation.

Vatistas (1986) experimentally observed that in the concentrated vortex, the azimuthal velocity component does not vary strongly in the axial direction. Therefore, with those assumptions the radial velocity component can be obtained from the $\theta-$momentum equation. This approaches Rankine model as a parameter denoting the sharpness of the velocity profile near the radius of the maximum wind increases infinitely (the details are given the main text). Vatistas et al. (1989) model is a generalization of a few well-known vortex tangential-velocity models. Vatistas et al. (1991) proposed the tangential velocity profiles for vortices with continuous distributions of flow quantities. Recently, Gillmeier et al. (2018) have reviewed some classical analytical tornado-like vortex flow field models.

The full scale structure of tornado is highly complex and therefore several issues such as instabilities, singularities and nonlinearity pop up to be addressed (Lewellen, 1993; Alexander and Wurman, 2008; Karstens et al., 2010). Hence, to understand the complete physical processes adhering to the tornado flow field, simplified mathematical models are required, which minimize the error existing in

the full-scale data observations and allow to explain original velocity and pressure fields. Collecting real wind field data from tornadoes in nature has been a difficult task for observers because of their destructive nature. Now-a-days researchers use Doppler radars for enabling full-scale tornado data from a safe distance. However, the data collected from such measurements are largely limited to the genesis of tornadoes (Bluestein et al., 1993, 2003, 2005; Lund and Snow, 1993; Wurman et al., 1996; Davies-Jones and Wood, 2006).

Ying and Chang (1970) opine, "Tornado is a huge vortex column with a low pressure visual core", and with this consideration Pandey and Maurya (2017) floated a mathematical model for atmospheric vortices by assuming an annular vortex. However, despite the fact that that the characteristics discovered hold for all whirlwinds, it was discussed in detail with regard to dust devils.

Baker and Sterling (2017) have recently published a paper in which for inviscid vortex flows they assumed the dimensionless radial velocity as $\overline{u} = -\frac{4\delta\overline{r}\overline{z}}{\left(1+\overline{r}^2\right)\left(1+\overline{z}^2\right)}$, where $\delta$ is the ratio between the vertical and horizontal length scales, and the rest bear the usual meaning. The other two components of velocity have been deduced as $\overline{v} = \frac{K\overline{r}\log\left(1+\overline{z}^2\right)}{\left(1+\overline{r}^2\right)}$ ($K$ being a constant) and $\overline{w} = \frac{4\delta\log\left(1+\overline{z}^2\right)}{\left(1+\overline{r}^2\right)^2}$ from the Euler equation. The viscous effects remained untouched.

With the objective to get new exact solutions to the equations governing dynamics of tornadoes duly considering viscous effects, we target to model single-cell tornadoes by considering radial velocity whose variation in vertical direction is consistent with the flow field in the laboratory vortex simulator (Ward, 1972). We aim to deduce vertical and azimuthal velocities and pressure as well with due consideration to the inferences made by Makarieva et al. (2011), who concluded, "The decrease of pressure along the vertical axis sustains the ascending air motion with vertical velocity $w$ and induces a compensating horizontal air inflow with radial

velocity $u$. The converging radial flow has maximal velocity at the surface, where the magnitude of the condensation-induced pressure drop is the largest. Radial velocity approaches zero at a certain height $z = h$, which approximately coincides with the cloud height".

## 6.2 The physical model and mathematical formulation

Equations governing the motion of a steady incompressible Newtonian viscous fluid with axial symmetry are given by

$$u\frac{\partial u}{\partial r} + w\frac{\partial u}{\partial z} - \frac{v^2}{r} = -\frac{1}{\rho}\frac{\partial p}{\partial r} + \nu\left\{\frac{\partial^2 u}{\partial r^2} + \frac{1}{r}\frac{\partial u}{\partial r} - \frac{u}{r^2} + \frac{\partial^2 u}{\partial z^2}\right\}, \tag{6.1}$$

$$u\frac{\partial v}{\partial r} + w\frac{\partial v}{\partial z} + \frac{uv}{r} = \nu\left\{\frac{\partial^2 v}{\partial r^2} + \frac{1}{r}\frac{\partial v}{\partial r} - \frac{v}{r^2} + \frac{\partial^2 v}{\partial z^2}\right\}, \tag{6.2}$$

$$u\frac{\partial w}{\partial r} + w\frac{\partial w}{\partial z} = -\frac{1}{\rho}\frac{\partial p}{\partial z} + \nu\left\{\frac{\partial^2 w}{\partial r^2} + \frac{1}{r}\frac{\partial w}{\partial r} + \frac{\partial^2 w}{\partial z^2}\right\} + F_z, \tag{6.3}$$

$$\frac{1}{r}\frac{\partial (ru)}{\partial r} + \frac{\partial w}{\partial z} = 0. \tag{6.4}$$

where $u$, $v$, $w$ are respectively the radial, azimuthal and vertical components of fluid velocity, and $r$, $z$ are the radial and axial coordinates; $p$ stands for the pressure, $\nu$ for the kinematic viscosity and $\rho$ for the density. The body forces (buoyancy) in the vertical direction are denoted by $F_z$.

Variables in Eqs. (6.1)-(6.4) are made dimensionless with primed notations as follows:

$$r' = \frac{r}{r_m},\ z' = \frac{z}{r_m},\ u' = \frac{u}{v_m},\ v' = \frac{v}{v_m},\ w' = \frac{w}{v_m},\ p' = \frac{p}{\rho v_m^2},\ F_z' = \frac{F_z}{v_m^2/r_m}. \tag{6.5}$$

where $r_m$ is the core radius and $v_m$ is the maximum azimuthal velocity.

In view of Eq. (6.5), Eqs. (6.1)−(6.4), on dropping the primes, are transformed to

$$u\frac{\partial u}{\partial r} + w\frac{\partial u}{\partial z} - \frac{v^2}{r} = -\frac{\partial p}{\partial r} + \frac{1}{Re}\left\{\frac{\partial^2 u}{\partial r^2} + \frac{1}{r}\frac{\partial u}{\partial r} - \frac{u}{r^2} + \frac{\partial^2 u}{\partial z^2}\right\}, \tag{6.6}$$

$$u\frac{\partial v}{\partial r} + w\frac{\partial v}{\partial z} + \frac{uv}{r} = \frac{1}{Re}\left\{\frac{\partial^2 v}{\partial r^2} + \frac{1}{r}\frac{\partial v}{\partial r} - \frac{v}{r^2} + \frac{\partial^2 v}{\partial z^2}\right\}, \tag{6.7}$$

$$u\frac{\partial w}{\partial r} + w\frac{\partial w}{\partial z} = -\frac{\partial p}{\partial z} + \frac{1}{Re}\left\{\frac{\partial^2 w}{\partial r^2} + \frac{1}{r}\frac{\partial w}{\partial r} + \frac{\partial^2 w}{\partial z^2}\right\} + F_z, \tag{6.8}$$

$$\frac{1}{r}\frac{\partial (ru)}{\partial r} + \frac{\partial w}{\partial z} = 0. \tag{6.9}$$

where $Re = r_m v_m/\nu$ denotes the Reynolds number.

### 6.2.1 Radial velocity

The winds blowing towards the centre of the tornado in the radial direction below few meters (or kms) of height, play a crucial role in the formation of tornadoes. We consider the radial velocity of the form $u(r, z) = -U(r)F(z)$, where $U(r)$ is a function of only $r$ and $F(z)$ is a function of only $z$, and the negative sign indicates that the radial wind blows towards the centre.

It is mostly considered that the strong inflow weakens along the radial direction and reduces to zero at the centre of the tornado. When the wind starts to rotate about the axis of rotation, it is physically accepted that the radial velocity diminishes with height and approaches zero at a certain height $z = h$, which approximately coincides with the cloud height (Makarieva et al., 2011).

We therefore assume that the radial velocity decreases linearly with height and vanishes at height $z = h$, i.e., $F(z) = 1 - az/h$, where the parameter a controls the shape of $F(z)$ and $a$ must be 1 when $z$ tends to $h$ so that $F(z)$ vanishes. This is consistent with the flow field in the laboratory vortex simulator (Ward, 1972 and Church et al., 1979). Hence, the radial velocity may be taken as

$$u(r,z) = -U(r)\left(1 - az/h\right), \ for\ 0 \leq z \leq h\ and\ u = 0\ h < z \leq H, \tag{6.10}$$

For one-cell tornado model, Burger (1948)-Rott (1958) considered the radial velocity proportional to radial distance, which is physically unacceptable because it has no upper bound in the radial direction.

In the opinion of Vatistas (1989), concentrated vortices produced in air and water follow a certain relationship. That relationship inspired Vatistas et al. (1991) to assume the tangential velocity (i.e. azimuthal velocity) of the form $v = r/\left(1 + r^{2\beta}\right)^{1/\beta}$, where $\beta$ governs the sharpness of the velocity profile near the radius of the maximum wind. $\beta \to \infty$, leads to Rankine's model. Smaller integral values of $\beta$ give smoother turns. Then with the assumption that the radial velocity does not depend strongly on the axial coordinates, Vatistas et al. (1991) derived from momentum conservation equation that the dimensionless radial velocity is $U(r) = -2(\beta+1)r^{(2\beta-1)}/\left(1 + r^{2\beta}\right)$. In that model, $U$ is well-behaved except for the numerical value of $\beta < 1$, where $U$ has a singularity near the tornado centre. For simple one-cell vortex, we accept it for $\beta = 1$, and so the dimensionless form of $U(r)$ is $U(r) = 4r/(1 + r^2)$. Thus, the final form of the radial velocity may be considered as

$$u(r,z) = -\frac{r}{(1+r^2)}\left(1 - a\frac{z}{h}\right), \tag{6.11}$$

where the second factor is based on the conclusion made by Makarieva et al. (2011); i.e., the pressure drop along the vertical axis sustains the ascending air motion with vertical velocity and induces a compensating horizontal air inflow with radial velocity. The converging radial flow has maximal velocity at the surface, where the magnitude of the condensation-induced pressure drop is the largest. $u \to 0$, at a certain height $z = h$, which is approximately the cloud height. Further, the coefficient 4 has been dropped as it does not modify the model qualitatively and further we shall be deriving other components from mass conservation and momentum conservation equations.

### 6.2.2 Vertical velocity

Substituting Eq. (6.11) into the continuity (6.9) with the consideration that $w(r, z) = w_1(r) \times w_2(z)$, we obtain the vertical velocity as

$$w(r, z) = \frac{2}{(1 + r^2)^2} \left\{ \left( z - a\frac{z^2}{2h} \right) + K \right\}, \tag{6.12}$$

where $K$ is an integrating constant and is determined by using the boundary condition that vertical velocity $w_2(z) = w_0$ at $z = 0$. This yields

$$w(r, z) = \frac{2}{(1 + r^2)^2} \left( w_0 + z - a\frac{z^2}{2h} \right). \tag{6.13}$$

### 6.2.3 Azimuthal velocity

#### 6.2.3.1 Inviscid flow

First of all, we investigate the flow field of a simple one-cell tornado vortex with high Reynolds number disregarding viscous terms. Under this consideration the azimuthal momentum equation (6.7) reduces as

$$u\left(\frac{\partial v}{\partial r}+\frac{v}{r}\right)+w\frac{\partial v}{\partial z}=0. \tag{6.14}$$

By applying the method of separation of variables, the azimuthal velocity is obtained as

$$v(r,z)=\frac{Cr^{\alpha-1}\left(w_0+z-a\frac{z^2}{2h}\right)^{\alpha/2}}{(1+r^2)^{\alpha/2}}, \tag{6.15}$$

where $C$ is an arbitrary constant and $\alpha$, a real number, is a separation constant. The azimuthal velocity is maximum at $r^2=\alpha-1$ and $z=h/a$. We may determine $C$ in terms of the swirl ratio $S=v_m/u_m$ at the reference height, $v_m$, $u_m$ being respectively the maximum azimuthal and maximum radial velocities. Consequently, $C=2aS/h$ and hence

$$v(r,z)=\frac{2aSr^{\alpha-1}\left(w_0+z-a\frac{z^2}{2h}\right)^{\alpha/2}}{h\,(1+r^2)^{\alpha/2}}, \tag{6.16}$$

A non-zero azimuthal velocity at $z=0$ at the ground level is a significant observation for real tornadoes.

#### 6.2.3.2 Viscous flow

Considering the vortex Reynolds number $Re$ very large (or equivalently, $\epsilon = Re^{-1} \ll 1$), we seek an asymptotic solution of Eq. (6.7) in the form

$$v(r,z) = v_0(r,z) + \epsilon v_1(r,z) + \epsilon^2 v_2(r,z) + ..., \tag{6.17}$$

assuming the series expansion to converge for higher orders of $\epsilon$. However, the entire calculation in this section will be carried out for $w_0 = 0$ as it simply augments the velocity to some extent without contributing in qualitative terms.

Substituting Eq. (6.17) into Eq. (6.7) and equating similar powers of $\epsilon$ on the two sides, we get the following equations corresponding to the zeroth and the first order of $\epsilon$ as follows:

$$\epsilon^0 : \; u\left(\frac{\partial v_0}{\partial r} + \frac{v_0}{r}\right) + w\frac{\partial v_0}{\partial z} = 0, \tag{6.18}$$

$$u\left(\frac{\partial v_1}{\partial r} + \frac{v_1}{r}\right) + w\frac{\partial v_1}{\partial z} = \left\{\frac{\partial^2 v_0}{\partial r^2} + \frac{1}{r}\frac{\partial v_0}{\partial r} - \frac{v_0}{r^2} + \frac{\partial^2 v_0}{\partial z^2}\right\}. \tag{6.19}$$

(Note: In order to avoid unnecessary derivations in view of very large Reynolds number, we evaluate the series only up to the first order of $\epsilon$.)

The solution of Eq. (6.18), which is under no perturbation, is the same as that of Eq. (6.15), i.e.

$$v_0(r,z) = \frac{Cr^{\alpha-1}\left(z - a\frac{z^2}{2h}\right)^{\alpha/2}}{(1+r^2)^{\alpha/2}}, \tag{6.20}$$

Further, in terms of angular momentum $M_1 = rv_1$, Eq. (6.19) may be reproduced as

$$u\frac{\partial M_1}{\partial r} + w\frac{\partial M_1}{\partial z} = f(r,z), \tag{6.21}$$

where

$$f(r,z) = C\left(z - a\frac{z^2}{2h}\right)^{\alpha/2}\frac{r^\alpha}{(1+r^2)^{\alpha/2}}\left[\left\{\frac{\alpha(\alpha-2)r^{-2}-4\alpha}{(1+r^2)^2}\right\} + \frac{\alpha}{2}\left(z - a\frac{z^2}{2h}\right)^{-2}\left\{\left(\frac{\alpha}{2}-1\right)\left(1-\frac{az}{h}\right)^2 - \frac{a}{h}\left(z - a\frac{z^2}{2h}\right)\right\}\right], \tag{6.22}$$

Eq. (6.21) is a first order linear inhomogeneous partial differential equation with variable coefficients. The Lagrange subsidiary equations will be therefore

$$\frac{dr}{-\frac{r}{(1+r^2)}\left(1-\frac{az}{h}\right)} = \frac{dz}{\frac{2}{(1+r^2)^2}\left(z-\frac{az^2}{2h}\right)} = \frac{dM_1}{f(r,z)}. \tag{6.23}$$

Considering the first equality, the first integral is obtained as

$$A\left(z - \frac{az^2}{2h}\right) = 1 + \frac{1}{r^2}, \tag{6.24}$$

and the second integral is obtained from the second equality

$$\frac{dz}{2\left(z-\frac{az^2}{2h}\right)} = \frac{dM_1}{(1+r^2)^2 f(r,z)},$$

which yields

$$
\begin{aligned}
&M_1(r,z) \qquad (6.25)\\
&= \frac{Cr^{\alpha}\left(z-a\frac{z^2}{2h}\right)^{\alpha/2}}{(1+r^2)^{\alpha/2}}\left[\frac{\alpha(\alpha-2)(1+r^2)z}{r^2\left(z-\frac{az^2}{2h}\right)}-\alpha(\alpha+2)\log\left(\frac{z}{1-\frac{az^2}{2h}}\right)+\frac{\alpha(\alpha-2)(1+r^2)^2}{4r^4\left(z-\frac{az^2}{2h}\right)^2}\times\right.\\
&\left\{\left(1-\frac{az}{h}\right)\log\left(1+\frac{1}{r^2}\right)+\frac{az}{h}\log\left(\frac{1}{r^2}\right)-r^2\left(1-\frac{az}{h}\right)+2\left\{1-\log\left(1-\frac{az}{2h}\right)\right\}-\right.\\
&\left.\left.\frac{1}{K_2}\left(\frac{r^2\left(z-\frac{az^2}{2h}\right)}{1+r^2}-\frac{h}{a}\right)\log\frac{\left(z-\frac{h}{a}\right)-k_2}{\left(z-\frac{h}{a}\right)+K_2}\right\}-\frac{\alpha h}{aK_2^3}\left\{\frac{\left(z-\frac{h}{a}\right)K_2}{K_2^2-\left(z-\frac{h}{a}\right)^2}+\log\left|\frac{\sqrt{K_2+\left(z-\frac{h}{a}\right)}}{\sqrt{K_2-\left(z-\frac{h}{a}\right)}}\right|\right\}\right]\\
&\quad+\phi\left(\frac{1+r^2}{r^2\left(z-\frac{az^2}{2h}\right)}\right),
\end{aligned}
$$

for $\frac{2h}{aA}-\frac{h^2}{a^2}=-K_2^2<0$.

where $\phi$ is an arbitrary function.

Hence, the azimuthal velocity up to the first order may be given by

$$
\begin{aligned}
v(r,z) = &\frac{Cr^{\alpha-1}\left(z-a\frac{z^2}{2h}\right)^{\alpha/2}}{(1+r^2)^{\alpha/2}}\\
&+\frac{1}{Re}\left[\frac{Cr^{\alpha}\left(z-a\frac{z^2}{2h}\right)^{\alpha/2}}{(1+r^2)^{\alpha/2}}\left\{\frac{\alpha(\alpha-2)(1+r^2)z}{r^2\left(z-\frac{az^2}{2h}\right)}-\alpha(\alpha+2)\log\left(\frac{z}{1-\frac{az^2}{2h}}\right)+\right.\right.\\
&\frac{\alpha(\alpha-2)(1+r^2)^2}{4r^4\left(z-\frac{az^2}{2h}\right)^2}\left\{\left(1-\frac{az}{h}\right)\log\left(1+\frac{1}{r^2}\right)+\frac{az}{h}\log\left(\frac{1}{r^2}\right)-r^2\left(1-\frac{az}{h}\right)+\right.\\
&2\left\{1-\log\left(1-\frac{az}{2h}\right)\right\}-\frac{1}{K_2}\left(\frac{r^2\left(z-\frac{az^2}{2h}\right)}{1+r^2}-\frac{h}{a}\right)\log\frac{\left(z-\frac{h}{a}\right)-k_2}{\left(z-\frac{h}{a}\right)+K_2}\Bigg\}-\\
&\left.\left.\frac{\alpha h}{aK_2^3}\left\{\frac{\left(z-\frac{h}{a}\right)K_2}{K_2^2-\left(z-\frac{h}{a}\right)^2}+\log\left|\frac{\sqrt{K_2+\left(z-\frac{h}{a}\right)}}{\sqrt{K_2-\left(z-\frac{h}{a}\right)}}\right|\right\}\right\}+\frac{1}{r}\phi\left(\frac{1+r^2}{r^2\left(z-\frac{az^2}{2h}\right)}\right)\Bigg],
\end{aligned}
\qquad (6.26)
$$

for $\frac{2h}{aA} - \frac{h^2}{a^2} = -K_2^2 < 0$.

(The involved details are given in Appendix $A$)

**Special Case**

The parameter $\alpha$ determines the shape of velocity profile. Baker and Sterling (2017) opine that in order to retain desirable forced vortex behavior at the tornado center, where velocity is proportional to radius, and free vortex behavior at large distances from the center, where velocity is inversely proportional to radius, we need to adopt $\alpha = 2$.

Further, the last term $\phi/r$ in Eq. (6.26) together with arbitrary function $\phi$ is a part of velocity and similar to the first term, so the appropriate term will be $r\left(z - az^2/2h\right)/(1+r^2)$. Hence, the azimuthal velocity may be appropriately put for $\alpha = 2$ in the form,

$$v(r,z) = \frac{Crz\left(1-\frac{az}{2h}\right)}{1+r^2}\left[1 - \frac{1}{Re}\left\{\gamma + 8\log\left(\frac{z}{1-\frac{az}{2h}}\right) + \frac{2h}{aK_2^3}\left\{\frac{\left(z-\frac{h}{a}\right)K_2}{K_2^2 - \left(z-\frac{h}{a}\right)^2} + \log\left|\frac{\sqrt{K_2 + \left(z-\frac{h}{a}\right)}}{\sqrt{K_2 - \left(z-\frac{h}{a}\right)}}\right|\right\}\right\}\right], \tag{6.27}$$

for $\frac{2h}{aA} - \frac{h^2}{a^2} = -K_2^2 < 0$, where $K_2 = \sqrt{\frac{h^2}{a^2} - \frac{2hr^2z\left(1-\frac{az}{2h}\right)}{a(1+r^2)}}$, $\gamma$ is an arbitrary constant. In view of very large Reynolds number, we evaluate $\gamma$ approximately in terms of $C$, determined for non-viscous case, so that $\gamma = Re\left(1 - \frac{2S}{C}\right) - 8\log\left(\frac{2h}{a}\right)$. Eq. (6.27) may therefore be given by

$$v(r,z) = \frac{rz\left(1-\frac{az}{2h}\right)}{1+r^2}\left[2S - \frac{C}{Re}\left\{8\log\left(\frac{az}{2h-az}\right) + \frac{2h}{aK_2^3}\left\{\frac{\left(z-\frac{h}{a}\right)K_2}{K_2^2 - \left(z-\frac{h}{a}\right)^2} + \log\left|\frac{\sqrt{K_2 + \left(z-\frac{h}{a}\right)}}{\sqrt{K_2 - \left(z-\frac{h}{a}\right)}}\right|\right\}\right\}\right], \tag{6.28}$$

With respect to the axial coordinates, the azimuthal velocity has parabolic profile.

### 6.2.4 Pressure

#### 6.2.4.1 Inviscid flow

Ignoring the viscous terms, the radial momentum equation in the dimensionless form reduces to

$$-\frac{\partial P}{\partial r} = u\frac{\partial u}{\partial r} + w\frac{\partial u}{\partial z} - \frac{v^2}{r}. \tag{6.29}$$

Substituting the expressions from Eqs. (6.11), (6.13) and Eq. (6.15) respectively for $u$, $w$ and $v$ into Eq. (6.29), we obtain the radial pressure gradient as

$$-\frac{\partial P}{\partial r} = \frac{r\left(1-r^2\right)}{\left(1+r^3\right)^3}\left(1-\frac{az}{h}\right)^2 + \frac{2ra}{h\left(1+r^2\right)^3}\left(z-\frac{az^2}{2h}\right) - \frac{C^2 r^{2\alpha-3}\left(z-\frac{az^2}{2h}\right)^\alpha}{\left(1+r^2\right)^\alpha}, \tag{6.30}$$

and integrating Eq. (6.30) with respect to $r$, the pressure as

$$P(r,z) = -\frac{r^3}{2\left(1+r^2\right)^2}\left(1-\frac{az}{h}\right)^2 + \frac{a}{2h\left(1+r^2\right)^2}\left(z-\frac{az^2}{2h}\right) + C^2\left(z-\frac{az^2}{2h}\right)^\alpha \times \int \frac{r^{2\alpha-3}}{\left(1+r^2\right)^\alpha} dr + f(z), \tag{6.31}$$

where $f(z)$ is the integrating function to be determined later.

Differentiating Eq. (6.31) with respect to $z$, the axial pressure gradient is given by

$$\frac{\partial P}{\partial z} = \left[\frac{a\left(2r^2+1\right)}{4h\left(1+r^2\right)^2} + C^2\alpha\left(z-\frac{az^2}{2h}\right)^{\alpha-1}\int\frac{r^{2\alpha-3}}{\left(1+r^2\right)^{\alpha}}dr\right]\left(1-\frac{az}{h}\right) + f^{'}(z), \tag{6.32}$$

#### 6.2.4.2 The buoyancy field

We write the axial momentum equation as

$$u\frac{\partial w}{\partial r} + w\frac{\partial w}{\partial z} = -\frac{\partial P}{\partial z} + F_z, \tag{6.33}$$

where $F_z$ denotes the buoyancy force per unit volume. Thus, substituting $u$ from Eq. (6.11), $w$ from Eq. (6.13) and the axial pressure gradient from Eq. (6.32) into Eq. (6.33), we obtain buoyancy as

$$\begin{aligned} F_z = &\left[\frac{4}{\left(1+r^2\right)^3}\left(z-\frac{az^2}{2h}\right) + \frac{a\left(1+2r^2\right)}{4h\left(1+r^2\right)^2} + C^2\alpha\left(z-\frac{az^2}{2h}\right)^{\alpha-1}\int\frac{r^{2\alpha-3}}{\left(1+r^2\right)^{\alpha}}dr\right] \\ &\times\left(1-\frac{az}{h}\right) + f^{'}(z), \end{aligned} \tag{6.34}$$

#### 6.2.4.3 Determination of pressure for viscous flow

Substituting $u$ from Eq. (6.11), $v$ from Eq. (6.28) and $w$ from Eq. (6.13) into Eq. (6.6), the radial pressure gradient may be given by

$$-\frac{\partial p}{\partial r} = \frac{r}{\left(1+r^2\right)^3}\left[\left(1-r^2\right)\left(1-\frac{az}{2h}\right)^2 + \frac{2a}{h}\left(z-\frac{az^2}{2h}\right) - \frac{8}{Re}\left(1-\frac{az}{h}\right)\right] - \frac{v^2}{r}, \tag{6.35}$$

which, on performing integration from 0 to $r$, gives

$$\begin{aligned} p(r,z)-p(0,z) = & -\frac{r^2}{2\left(1+r^2\right)^2}\left(1-\frac{az}{h}\right)^2 \\ & +\frac{1}{2}\left\{1-\frac{1}{\left(1+r^2\right)^2}\right\}\left\{\frac{a}{h}\left(z-\frac{az^z}{2h}\right)-\frac{4}{Re}\left(1-\frac{az}{h}\right)\right\} \\ & +\int_0^r \frac{v^2(r,s)}{s}ds. \end{aligned} \tag{6.36}$$

Similarly, from Eqs. (6.11), (6.13) and Eq. (6.8), the axial pressure gradient may be obtained as

$$-\frac{\partial p}{\partial z}+F_z = \left(z-\frac{az^2}{2h}\right)\frac{4}{\left(1+r^2\right)^4}\left\{\left(1-\frac{az}{h}\right)\left(1+2r^2\right)+\frac{4\left(1-2r^2\right)}{Re}\right\}+\frac{2a}{Reh\left(1+r^2\right)^2}, \tag{6.37}$$

integration of which from 0 to $z$, yields

$$\begin{aligned} p(r,z)-p(r,0) = & -\frac{4}{\left(1+r^2\right)^4}\left\{\frac{\left(1+2r^2\right)}{2}\left(z-\frac{az^2}{2h}\right)^2+\right. \\ & \left.\frac{2\left(1-2r^2\right)}{Re}\left(z^2-\frac{az^3}{3h}\right)\right\}-\frac{2a}{Reh\left(1+r^2\right)^2}+\int_0^z F_s ds, \end{aligned} \tag{6.38}$$

From Eq. (6.38) at $r=0$, we get

$$p(0,z) = p(0,0)-2\left\{\left(z-\frac{az^2}{2h}\right)^2+\frac{4}{Re}\left(z^2-\frac{az^3}{3h}\right)\right\}-\frac{2az}{Re\,h}+\int_0^z F_s(0,s)ds, \tag{6.39}$$

Substituting Eq. (6.39) into Eq. (6.36), we get pressure given by

$$\begin{aligned} p(r,z) - p(0,0) = & -\frac{r^2}{2\left(1+r^2\right)^2}\left(1-\frac{az}{h}\right)^2 \\ & + \frac{1}{2}\left\{1-\frac{1}{\left(1+r^2\right)^2}\right\}\left\{\frac{a}{h}\left(z-\frac{az^2}{2h}\right)-\frac{4}{Re}\left(1-\frac{az}{h}\right)\right\} \\ & + \int_0^r \frac{v^2(s,z)}{s}ds - \left\{2\left(z-\frac{az^2}{2h}\right)^2+\frac{8}{Re}\left(z^2-\frac{az^3}{3h}\right)\right\} \\ & - \frac{2az}{Re\ h} + \int_0^z F_s(0,s)ds. \end{aligned} \tag{6.40}$$

## 6.3 Results and discussions

The present model is more general in the sense that all the three components are also dependent on the axial coordinate. The derived velocity components are plotted to study the radial and axial profiles and the impact of viscosity thereon.

### 6.3.1 Radial component of velocity

Radial dependence of the radial component of velocity was assumed of the form based on the empirical model of Vatistas et al. (1991) for viscous flow. The form was extended for axial dependence as per the suggestions of Makarieva et al. (2011). The dimensionless radial velocity profile at fixed axial distances are displayed in Fig. 6.1. The negative sign is an indication that the flow is inward. It is observed that the magnitude of the radial velocity increases to the maximum at the core but reverses the trend beyond and vanishes as it reaches the centre line. The magnitude reduces linearly with axial distance as per the supposition. The results are comparable with those obtained by Baker and Sterling (2017) who worked on inviscid flows but got

similar results for the dimensionless radial velocity with a different modification (Eq. (3) and Fig. 1*a* in Baker and Sterling, 2017) for the axial as well as radial dependence of the radial component. The radial component increases in magnitude until it reaches the core, but beyond that, they too mention that for large radius the radial component of velocity approaches zero as is required. This is to be noted that the radial and axial components have no viscous terms.

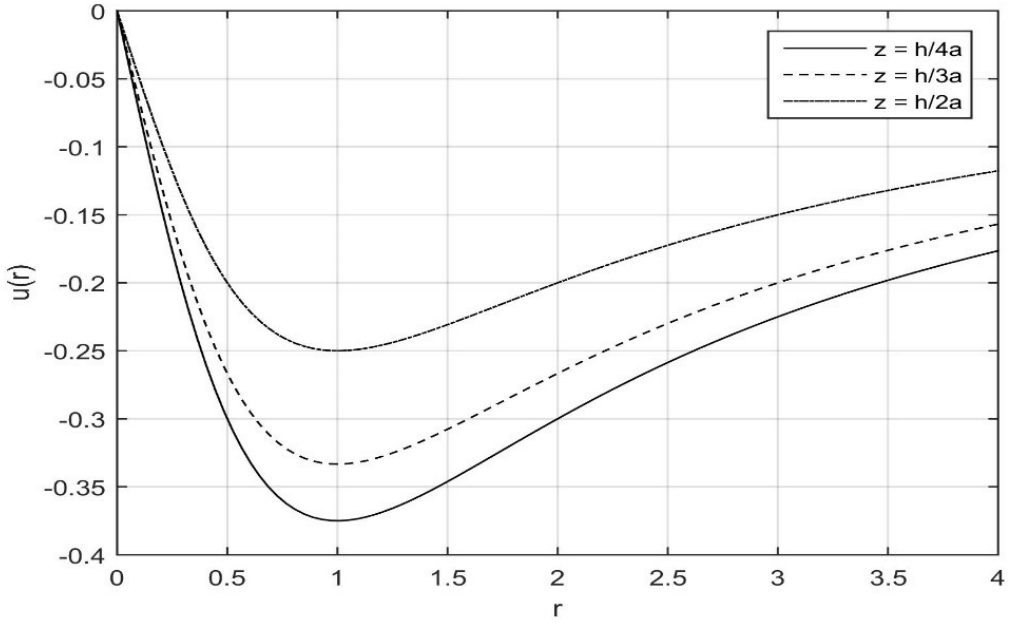


**Figure 6.1:** The radial profile of the radial component $u(r)$ of velocity based on Eq. (6.11). The parameters assumed here for the diagram are $h = 50$, and $a = 1$.

### 6.3.2 Vertical component of velocity

The vertical component of velocity has been derived from the continuity equation with substitution of the radial component designed in subsection (6.2.1). The plots are given in Figs. 6.2.

The radial profile of the axial component of velocity reveals that it is maximum at the centre line, weakens as we move radially outward, reduces at large distances from the axis and then vanishes gradually (Fig. 6.2*a*). Baker and Sterling (2017) have showed very similar results with their derived dimensionless vertical velocity.

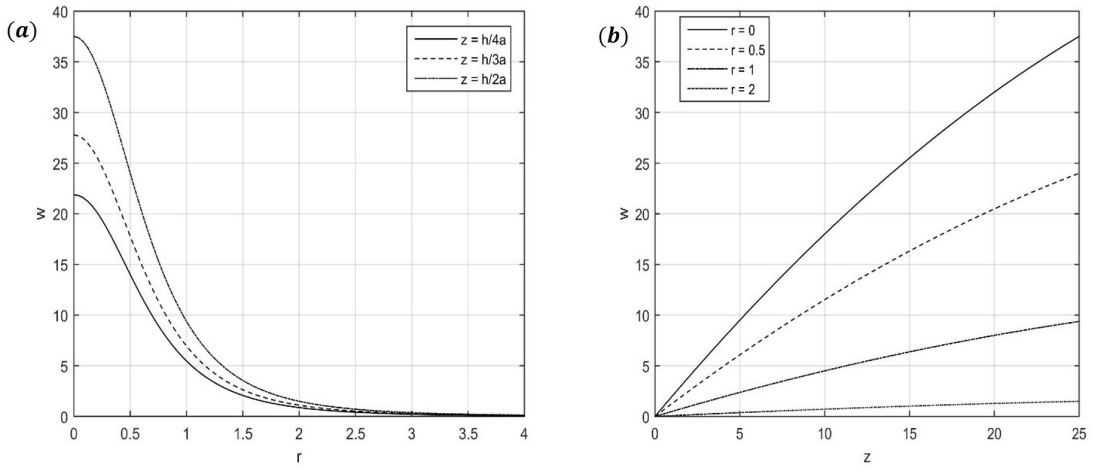


**Figure 6.2:** (*a*) The radial profile of the vertical velocity $w$ and (*b*) the dependence of $w$ on $z$. The plots are based on Eq. (6.13) and the parameters assumed here for the diagram are $h = 50$, and $a = 1$.

Vertical velocity increases along the axis (Fig. 6.2*b*). However, it diminishes as we move outward from the centre. Similar patterns with similar radial profiles were observed by Liu and Ishihara (2016) in their numerical study for tornadoes with swirl ratio 0.02 for weak vortices. As swirl ratio is not a parameter in our formula, it is not possible to compare with other observations or results given in that paper. Therefore, a further improvement is required considering some other aspects of the vortex motion.

### 6.3.3 Azimuthal component of velocity

The azimuthal velocity is the most significant component in a whirling motion. In this investigation, it has been derived on the basis of the assumption made for the radial component and also the axial component which was derived from the continuity equation by the substitution of the radial component of velocity. Unlike this, most of the previous theoretical investigations showed its dependence on the radial coordinate only ignoring its obvious variation in the axial direction. However, during numerical simulation, this fact could not be ruled out. Duly considering this aspect, Tang et al., (2018) simulated azimuthal velocity for various fixed values of axial coordinates and found it to match relatively less general models of Rankine (1882) and Burgers (1948)- Rott (1958). As an exception to the most of the previous results, Baker and Sterling (2017) have formulated the radial as well as axial dependence of the azimuthal velocity but for inviscid flows (Eq. 9 and Fig. 1*b* in Baker and Sterling, 2017). The results they obtained is similar to those of our model for inviscid part. However, the impact of viscosity cannot be compared. As both the models are based on model (Vatistas, 1991) in terms of the radial component, the observations are alike. Graphs given in the following paragraph reveal more.

Taking care of axial dependence of the azimuthal component of velocity, we draw plots showing its radial and axial profiles (Fig. 6.3). This component is strongest at the core, and inside and outside the core, it diminishes. This is revealed in the plots drawn. The radial profile has resemblance with simulated models of Tang et al., (2018), and the vertical profile is parabolic even for viscous flows, obvious from the constructed model given by the (Vatistas, 1989) for high Reynolds numbers.

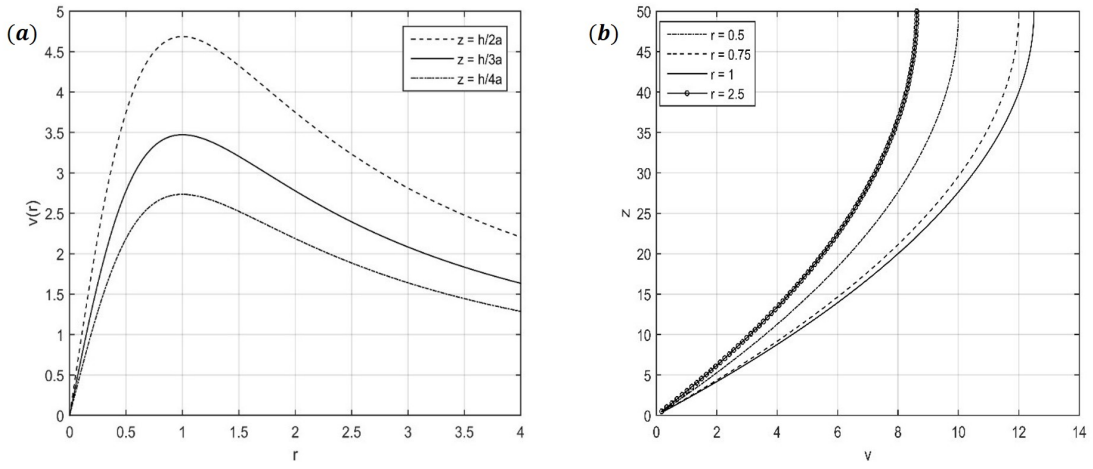


**Figure 6.3:** Plots for $(a)$ the radial profile of the azimuthal velocity $v$ and $(b)$ the dependence of $v$ on $z$. The plots are based on Eq. (6.28) and the parameters assumed here for the diagram are $S = 0.50$, $h = 50$ and $a = 1$.

In order to examine the impact of viscosity, we further draw some plots for different values of Reynolds number. We fix $S = 0.98$; i.e., the azimuthal and radial velocities are almost the same at their maxima. The radial length is varied in the range $r = 0.5 - 3.0$. We take the following three different cases and plot axial profiles of the azimuthal component of velocity:

**(a)** $r = 1.0$: This is the core where the velocity is maximum. Plots are drawn for $Re = 5, 10, 100, 10000$. The plots, drawn in Fig. 6.4, show that larger the Reynolds number, lesser is the velocity. However, once $Re = 100$, further increase in Reynolds number has insignificant impact as we observe that curves corresponding to $Re = 100 - 10000$ almost coincide.

**(b)** $r = 0.5$: This is a point inside the core and plots are drawn for $Re = 10, 100, 10000$. The trends are reversed. Larger the Reynolds number, lesser is the velocity.

**(c)** $r = 3.0$: This is a point outside the core and plots are drawn for $Re = 10, 100, 10000$. Beyond the core, the azimuthal velocity decreases. The trends for

the Reynolds number are similar to that inside the core, i.e. larger the Reynolds number, lesser is the velocity.

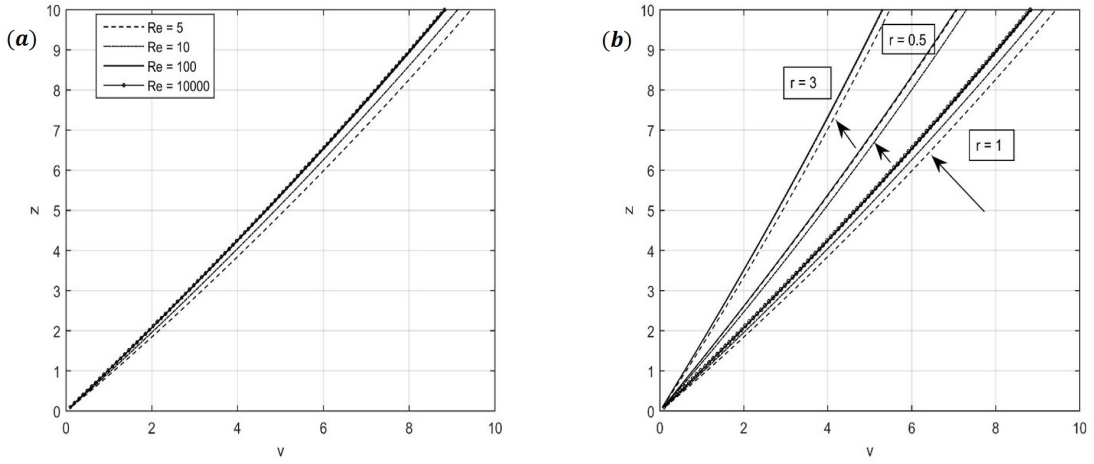


**Figure 6.4:** Plots for vertical profiles of the azimuthal velocity $v$ based on Eq. (6.28). The parameters assumed here for the diagram are $S = 0.98$, $h = 50$ and $a = 1$.

### 6.3.4 Pressure distribution

Radial pressure distributions for different axial positions are shown in Fig. 6.5($a$). We set $z = h/2a,\ h/3a,\ h/4a$ and $Re = 10000$. Profiles are similar to theoretical observation of Arsen'yev et al. (2011) and numerically simulated observation of Tang et al., (2018). That is, as we move outward from the axis, pressure increases, and also that pressure decreases as height increases. The drop from the circumferential pressure to the pressure at the axis, based on Eq. (6.36), increases with height for swirl ratio $S = 0.98$, or, in other words, the pressure at the axis, i.e, $p(0, z)$, is minimum. Plots are differently drawn in Fig. 6.5($b$), in which axial distribution of pressure, based on Eq. (6.38), has been plotted for different radial distances. The pressure is observed to fall as height is scaled; in other words, i.e. $p(r, 0)$, is maximum. If we fix $z$, trends are similar to what is observed in Fig. 6.5($a$). Further,

pressure drop becomes more in magnitude with height. This is a combined effect of the two observations.

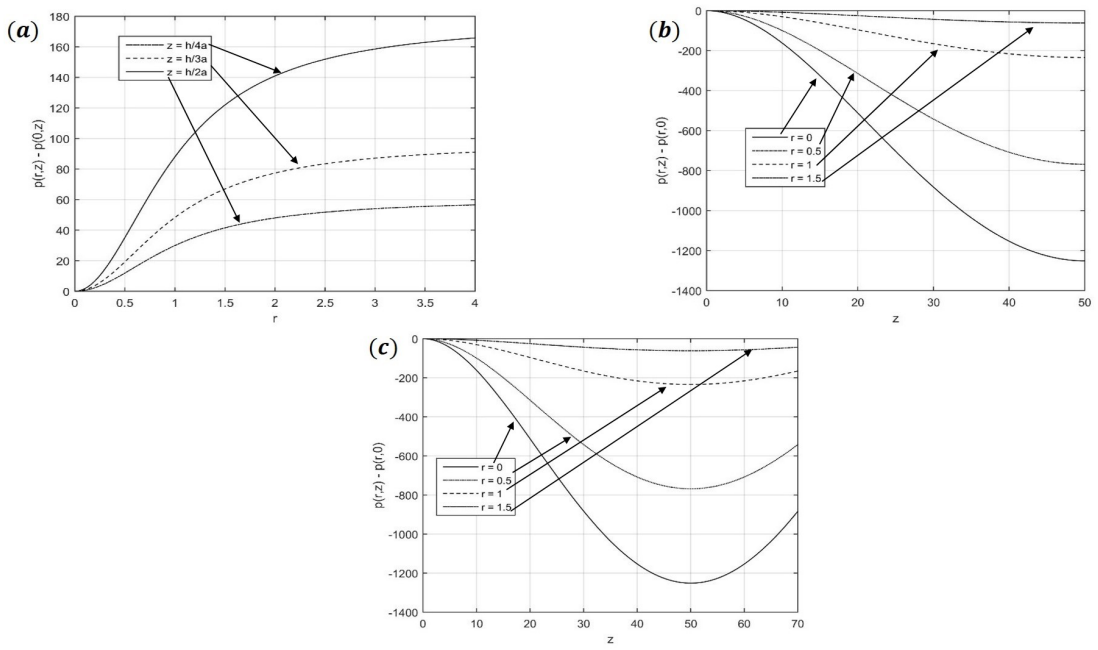


**Figure 6.5:** $(a)$ The radial distribution of pressure difference $p(r,z) - p(0,z)$ based on Eq. (6.36). $(b)$ The axial distribution of pressure difference $p(r,z) - p(r,0)$ based on Eq. (6.38) with $S = 0.98$ and $(c)$ The axial distribution of pressure difference $p(r,z) - p(r,0)$ based on Eq. (6.38) with $S = 0.15$. The other parameters assumed here for the diagrams are $h = 50$ and $a = 1$.

However, for $S = 0.15$ (i.e. the value Wang et al., 2017 talk about), the trends for pressure drop, shown in Fig. 6.5$(c)$, are similar to what Wang et al. (2017) observed in an experimental investigation, i.e., for some height pressure decreases (i.e, pressure drop increases in magnitude) while above that the trend gets reversed. However, it needs to be noted that neither we talk of roughness nor has it anything to do with roughness of the surface; this is just based on the model we have formulated. This is an indication that the swirl ratio plays a big role. Tang et al. (2018) have discussed this in detail.

In order to examine the effect of viscosity, we study pressure against different Reynolds numbers. The plots are given in Fig. 6.6. Pressure decreases with rising Reynolds number uniformly for all radial distances. This is an indication that quantitative difference in pressure is large between viscous and inviscid flows. Thus, an approximation, from viscous to inviscid flow, does not look fair; it will be difficult to fit experimental data with theoretical inviscid models.

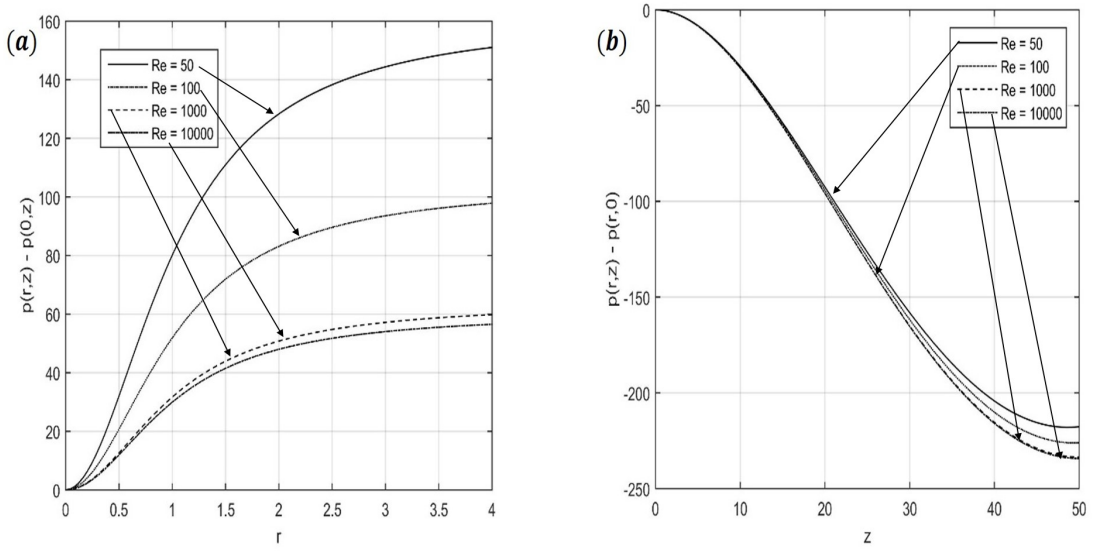


**Figure 6.6:** $(a)$ The radial distribution of pressure difference $p(r,z) - p(0,z)$ based on Eq. (6.36) with $z = h/4a$. $(b)$ The axial distribution of pressure difference $p(r,z) - p(r,0)$ based on Eq. (6.38). The other parameters assumed here for the diagrams are $S = 0.50$, $h = 50$, $a = 1$ and $r = 1$.

## 6.4 Conclusions

New results are mainly related to axial dependence of the various components of velocity. Although all the three components are functions of radial and axial coordinates, viscosity affects the azimuthal velocity and the pressure.

It is observed that the magnitude of the radial velocity increases to the maximum at the core but reverses the trend beyond and vanishes as it reaches the centreline. The magnitude reduces linearly with axial distance as per the supposition.

At the core, larger the Reynolds number, the lesser is the velocity for moderate Reynolds number. For larger Reynolds number, insignificant impact is observed. However, Inside and outside the core, the trends are reversed; i.e., larger the Reynolds number, lesser is the velocity.

Radial pressure distributions for different axial positions are similar to theoretical, experimental and numerical observations as given in the discussion. As we move outwards from the axis, pressure increases, but pressure decreases with height. Further, drop of pressure from the circumference to the axis increases in magnitude with height.

Pressure decreases with rising Reynolds number uniformly for all radial distances. This is an indication that quantitative difference in pressure is large between viscous and inviscid flows.

# Appendix A

In terms of angular momentum $M_1 = rv_1$, Eq. (6.19) is transformed to

$$u\frac{\partial M_1}{\partial r} + w\frac{\partial M_1}{\partial z} = f(r, z), \tag{A1}$$

where $f(r, z)$ has been given by Eq. (6.22).

Eq. $(A1)$ is a first order linear inhomogeneous partial differential equation with

variable coefficients. The Lagrange subsidiary equations are therefore given by

$$\frac{dr}{-\frac{r}{(1+r^2)}\left(1-a\frac{z}{h}\right)} = \frac{dz}{\frac{2}{(1+r^2)^2}\left(z-a\frac{z^2}{2h}\right)} = \frac{dM_1}{f(r,z)}, \tag{A2}$$

The first integral is obtained by considering the first equality, which is

$$A\left(z-a\frac{z^2}{2h}\right) = 1+\frac{1}{r^2}, \tag{A3}$$

where $A$ is an integration constant; and the second integral is obtained from the second equality

$$\frac{dz}{2\left(z-a\frac{z^2}{2h}\right)} = \frac{dM_1}{(1+r^2)^2 f(r,z)}, \tag{A4}$$

which gives

$$M_1(r,z) = \frac{C}{A^{\alpha/2}}\left[\alpha A(\alpha-2)z - \alpha(\alpha+2)\log\left(\frac{z}{1-a\frac{z}{h}}\right) + \frac{\alpha A^2\left(\frac{\alpha}{2}-1\right)}{2}I_1 - \frac{a\alpha A^2}{2h}I_2\right] + B, \tag{A5}$$

where $B$ is a function of $A$ and

$I_1 = \int \frac{\left(1-\frac{az}{h}\right)^2}{\left\{A\left(z-a\frac{z^2}{2h}\right)-1\right\}^2\left(z-a\frac{z^2}{2h}\right)}dz$, and $I_2 = \int \frac{1}{\left\{A\left(z-a\frac{z^2}{2h}\right)-1\right\}^2}dz$

which on performing integrations are as follows:

$(a)$ For $\frac{2h}{ah} - \frac{h^2}{a^2} = K_1^2 > 0$

$$I_1 = \left(1-\frac{az}{h}\right)\log\left\{A\left(z-a\frac{z^2}{2h}\right)\right\} + \frac{az}{h}\log\left\{A\left(z-a\frac{z^2}{2h}\right)-1\right\} - \frac{\left(1-a\frac{z}{h}\right)}{\left\{A\left(z-a\frac{z^2}{2h}\right)-1\right\}} + 2\left\{1-\log\left(1-\frac{az}{2h}\right)\right\} - \frac{2\left(1-\frac{Ah}{a}\right)}{AK_1}\arctan\left\{\frac{z-\frac{h}{a}}{K_1}\right\}, \tag{A6}$$

$$I_2 = \frac{2h^2}{a^2A^2K_1^3}\left[\frac{K_1\left(z-\frac{h}{a}\right)}{\left(z-\frac{h}{a}\right)^2+K_1^2} + \arctan\left\{\frac{z-\frac{h}{a}}{K_1}\right\}\right], \tag{A7}$$

(*b*) For $\frac{2h}{ah} - \frac{h^2}{a^2} = -K_2^2 < 0$

$$I_1 = \left(1 - \frac{az}{h}\right) \log\left\{A\left(z - a\frac{z^2}{2h}\right)\right\} + \frac{az}{h} \log\left\{A\left(z - a\frac{z^2}{2h}\right) - 1\right\} - \frac{\left(1 - a\frac{z}{h}\right)}{\left\{A\left(z - a\frac{z^2}{2h}\right) - 1\right\}} + 2\left\{1 - \log\left(1 - \frac{az}{2h}\right)\right\} - \frac{\left(1 - \frac{Ah}{a}\right)}{AK_2} \log\left\{\frac{\left(z - \frac{h}{a}\right) - K_2}{\left(z - \frac{h}{a}\right) + K_2}\right\}, \tag{A8}$$

$$I_2 = \frac{2h^2}{a^2A^2K_2^3}\left[\frac{K_2\left(z - \frac{h}{a}\right)}{K_2^2 - \left(z - \frac{h}{a}\right)^2} + \log\left|\frac{\sqrt{K_2 + \left(z - \frac{h}{a}\right)}}{\sqrt{K_2 - \left(z - \frac{h}{a}\right)}}\right|\right]. \tag{A9}$$

Substituting $I_1$ and $I_2$ from Eqs. $(A6)$, $(A7)$ into Eq. $(A5)$ and also using Eq. $(A3)$, for the case $(a)$, we get

$$M_1 = \frac{Cr^\alpha\left(z - a\frac{z^2}{2h}\right)^{\alpha/2}}{(1+r^2)^{\alpha/2}}\left[\frac{\alpha(\alpha-2)(1+r^2)z}{r^2\left(z - a\frac{z^2}{2h}\right)} - \alpha(\alpha+2)\log\left(\frac{z}{1 - a\frac{z}{2h}}\right) + L + \psi\right] + \phi\left(\frac{(1+r^2)}{r^2\left(z - a\frac{z^2}{2h}\right)}\right), \tag{A10}$$

where

$$L = L_1\left[\left(1 - \frac{az}{h}\right)\log\left(1 + \frac{1}{r^2}\right) + \frac{az}{h}\log\left(\frac{1}{r^2}\right) - r^2\left(1 - \frac{az}{h}\right) + 2\left\{1 - \log\left(1 - \frac{az}{2h}\right)\right\} - A_1\right]$$

$$L_1 = \frac{\alpha(\alpha-2)(1+r^2)^2}{4r^4\left(z - a\frac{z^2}{2h}\right)},\ A_1 = \frac{2}{K_1}\left(\frac{r^2\left(z - a\frac{z^2}{2h}\right)}{1+r^2} - \frac{h}{a}\right)\arctan\left(\frac{z - \frac{h}{a}}{K_1}\right),$$

and

$$\psi = -\frac{\alpha h}{aK_1^3}\left[\frac{K_1\left(z - \frac{h}{a}\right)}{\left(z - \frac{h}{a}\right)^2 + K_1^2} + \arctan\left(\frac{z - \frac{h}{a}}{K_1}\right)\right].$$

Similarly, for the case $(b)$, we get

$$M_1 = \frac{Cr^{\alpha}\left(z - a\frac{z^2}{2h}\right)^{\alpha/2}}{(1+r^2)^{\alpha/2}}\left[\frac{\alpha(\alpha-2)(1+r^2)z}{r^2\left(z - a\frac{z^2}{2h}\right)} - \alpha(\alpha+2)\log\left(\frac{z}{1-a\frac{z}{2h}}\right) + N + \psi\right] + \phi\left(\frac{(1+r^2)}{r^2\left(z - a\frac{z^2}{2h}\right)}\right), \tag{A11}$$

where

$$N = L_1\left[\left(1-\frac{az}{h}\right)\log\left(1+\frac{1}{r^2}\right) + \frac{az}{h}\log\left(\frac{1}{r^2}\right) - r^2\left(1-\frac{az}{h}\right) + 2\left\{1-\log\left(1-\frac{az}{2h}\right)\right\} - B_1\right]$$

$$L_1 = \frac{\alpha(\alpha-2)(1+r^2)^2}{4r^4\left(z - a\frac{z^2}{2h}\right)},\ B_1 = \frac{1}{K_2}\left(\frac{r^2\left(z - a\frac{z^2}{2h}\right)}{1+r^2} - \frac{h}{a}\right)\log\left\{\frac{\left(z-\frac{h}{a}\right) - K_2}{\left(z-\frac{h}{a}\right) + K_2}\right\},$$

and

$$\psi_1 = -\frac{\alpha h}{aK_2^3}\left[\frac{K_2\left(z-\frac{h}{a}\right)}{K_2^2 - \left(z-\frac{h}{a}\right)^2} + \log\left|\frac{\sqrt{K_2 + \left(z-\frac{h}{a}\right)}}{\sqrt{K_2 - \left(z-\frac{h}{a}\right)}}\right|\right].$$

Hence,

$(a)$ For $\frac{2h}{ah} - \frac{h^2}{a^2} = K_1^2 > 0$

$$V_1 = \frac{Cr^{\alpha-1}\left(z - a\frac{z^2}{2h}\right)^{\alpha/2}}{(1+r^2)^{\alpha/2}}\left[\frac{\alpha(\alpha-2)(1+r^2)z}{r^2\left(z - a\frac{z^2}{2h}\right)} - \alpha(\alpha+2)\log\left(\frac{z}{1-a\frac{z}{2h}}\right) + L + \psi\right] + \frac{1}{r}\phi\left(\frac{(1+r^2)}{r^2\left(z - a\frac{z^2}{2h}\right)}\right), \tag{A12}$$

where

$$L = L_1 \left[ \left(1 - \frac{az}{h}\right) \log\left(1 + \frac{1}{r^2}\right) + \frac{az}{h} \log\left(\frac{1}{r^2}\right) - r^2 \left(1 - \frac{az}{h}\right) + 2\left\{1 - \log\left(1 - \frac{az}{2h}\right)\right\} - A_1 \right]$$

$$L_1 = \frac{\alpha(\alpha-2)(1+r^2)^2}{4r^4\left(z - a\frac{z^2}{2h}\right)},\ A_1 = \frac{2}{K_1}\left(\frac{r^2\left(z - a\frac{z^2}{2h}\right)}{1+r^2} - \frac{h}{a}\right) \arctan\left(\frac{z - \frac{h}{a}}{K_1}\right),$$

and

$$\psi = -\frac{\alpha h}{a K_1^3}\left[\frac{K_1\left(z - \frac{h}{a}\right)}{\left(z - \frac{h}{a}\right)^2 + K_1^2} + \arctan\left(\frac{z - \frac{h}{a}}{K_1}\right)\right].$$

(*b*) For $\frac{2h}{ah} - \frac{h^2}{a^2} = -K_2^2 < 0$

$$v_1 = \frac{C r^{\alpha-1}\left(z - a\frac{z^2}{2h}\right)^{\alpha/2}}{(1+r^2)^{\alpha/2}}\left[\frac{\alpha(\alpha-2)(1+r^2)z}{r^2\left(z - a\frac{z^2}{2h}\right)} - \alpha(\alpha+2)\log\left(\frac{z}{1 - a\frac{z}{2h}}\right) + N + \psi\right] + \frac{1}{r}\phi\left(\frac{(1+r^2)}{r^2\left(z - a\frac{z^2}{2h}\right)}\right), \tag{A13}$$

where

$$N = L_1\left[\left(1 - \frac{az}{h}\right)\log\left(1 + \frac{1}{r^2}\right) + \frac{az}{h}\log\left(\frac{1}{r^2}\right) - r^2\left(1 - \frac{az}{h}\right) + 2\left\{1 - \log\left(1 - \frac{az}{2h}\right)\right\} - B_1\right]$$

$$L_1 = \frac{\alpha(\alpha-2)(1+r^2)^2}{4r^4\left(z - a\frac{z^2}{2h}\right)},\ B_1 = \frac{1}{K_2}\left(\frac{r^2\left(z - a\frac{z^2}{2h}\right)}{1+r^2} - \frac{h}{a}\right)\log\left\{\frac{\left(z - \frac{h}{a}\right) - K_2}{\left(z - \frac{h}{a}\right) + K_2}\right\},$$

and

$$\psi_1 = -\frac{\alpha h}{a K_2^3}\left[\frac{K_2\left(z - \frac{h}{a}\right)}{K_2^2 - \left(z - \frac{h}{a}\right)^2} + \log\left|\frac{\sqrt{K_2 + \left(z - \frac{h}{a}\right)}}{\sqrt{K_2 - \left(z - \frac{h}{a}\right)}}\right|\right].$$

**********